A Numerical Study of Instability Control for the Design of an Optimal Policy of Enhanced Oil Recovery by Tertiary Displacement Processes

Prabir Daripa · Xueru Ding

Abstract   In this paper, we consider the problem of control of hydrodynamic instability arising in the displacement processes during enhanced oil recovery by SP-flooding (Surfactant–Polymer). In particular, we consider a flooding process involving displacement of a viscous fluid in porous media by a less viscous fluid containing polymer and surfactant over a finite length which in turn is displaced by a even less viscous fluid such as water. The maximum stabilization capacities of several monotonic and non-monotonic viscous profiles created by non-uniform polymer concentration are studied in the presence of interfacial tensions created by surfactants. The study has been carried out numerically to determine and characterize the most optimal viscous profiles of each family. Similarities in optimal monotonic viscous profiles of this constant-time injection policy and other injection policies by previous workers are noted. The presence of interfacial instability (due to viscosity jump) and layer instability (due to viscosity gradient) in appropriate proportions has been numerically demonstrated to be a necessary condition for monotonic as well as optimal non-monotonic profiles except in the limiting case of infinite time injection in which case maximum stabilization appears to result from pure layer instability. It has also been demonstrated numerically that the optimal non-monotonic viscous profiles can have better stabilization potential than the optimal monotonic profiles. Many other new features of this injection policy which have not been recognized before have been discussed.

Keywords   Optimal viscous profile · Enhanced chemical oil recovery · Porous media flows · Linear stability

P. Daripa (✉)
Department of Mathematics, Texas A&M University, College Station, TX 77843, USA
e-mail: prabir.daripa@math.tamu.edu

X. Ding
Department of Petroleum Engineering, Texas A&M University at Qatar, Doha, Qatar

🖄 Springer

1 Introduction

In oil recovery by secondary displacement process, viscous oil in porous media is displaced by the injection of another less viscous fluid, usually water. It is well known that this displacement process is unstable when the displacing fluid has a lower viscosity than the displaced one. The essence of this instability is easily explained and analyzed when this porous media flow is viewed macroscopically by assuming existence of a front between displacing and displaced fluids. This viewpoint brings this porous media flow closer to Hele-Shaw flow, i.e., the displacement process taking place in a Hele-Shaw cell. A Hele-Shaw cell is a device consisting of two parallel plates separated by a distance 'b' very small in comparison to other two dimensions of the plates. Both of these flows are governed by Darcy's law: $\nabla p = -\mu \mathbf{v}$ where p is the pressure, $\mathbf{v}$ is the displacement velocity (an average of flow velocity between the parallel plates in case of Hele-Shaw cell), and μ is the viscosity of the fluid divided by permeability ($(b^2/12)$ in case of Hele-Shaw cell). Instability of the sharp front in this secondary displacement process, now known as Saffman–Taylor–Chouke instability, has been studied by Saffman and Taylor (1958) and Chouke et al. (1959). Because of this analogy and for obvious reasons which we will see later, below we make no distinction between a front and an interface and use these words interchangeably to mean the same entity.

It is worth mentioning here that the above analogy between porous media and Hele-Shaw flows is not without debate and for a valid reason. There are certainly some flaws in this analogy which is alluded to in this paragraph. Immiscible fluids as they flow in porous media are separated by interfaces at microscale that ideally can not be captured by a macroscopic interface without perhaps some capillary pressure dependence functionals. Current state of knowledge in this area does not provide any such appropriate functionals. In light of this, perhaps modeling motion of collection of such microscopic interfaces by a macroscopic interface is not so inappropriate when the goal is to gain an understanding of the interplay of various interfacial modes and layer (or fingering) modes. Moreover, the current study models correctly such immiscible fluid flow instabilities in Hele-Shaw cells.

One of the factors that has been known to degrade oil recovery is this viscosity driven Saffman–Taylor–Chouke instability. Therefore, oil recovery can be improved if a flooding process can be devised that will contain this instability. There are also other factors associated with wettability, capillary pressure, etc., that influence oil recovery. The objective in enhanced oil recovery process is to improve oil recovery by controlling these and other factors. Since there is an ever-increasing high demand and the growing shortage in supply of oil, a variety of specific processes which lead to improved recovery efficiency are under intensive study around the world today. One of the enhanced oil recovery (EOR) methods is ASP-flooding in which an aqueous phase containing alkali, polymer, and surfactant is used as one of the displacing fluids which may be followed by a sequence of other fluids having desirable properties. Polymer is used to increase the viscosity and surfactant is used to reduce the capillary pressure. Alkali is used primarily to generate in-situ surfactant to compensate for its depletion due to its adsorption into the rock matrix of the porous media. Shah and Schecter (1977) describes in detail many of the processes involved in ASP-flooding that lead to improved oil recovery than otherwise possible. This is a type of EOR which is of interest in this paper. Our study here will be mainly focused on modeling the effect of interfacial surfactants and polymer on stabilization of the advancing front sweeping the oil in a three-layer set-up where the ASP-flooding is followed by water flooding. The role of alkali will be, however, neglected in our study.

In the design of EOR processes based on stabilization (i.e., reducing the maximum growth rate of instability), dispersion relation is one of the key components that should partly guide

such design processes. The well-known dispersion relation $\sigma_{st}(k)$ of this advancing interfacial instability in a simpler two-layer flow with water displacing oil in secondary recovery is given by

$$\sigma_{st} = \frac{Uk(\mu_r - \mu_l) - k^3 T}{\mu_r + \mu_l}, \tag{1}$$

where subscript 'st' stands for Saffman–Taylor–Chouke instability, μ_r is the viscosity of the displaced fluid, μ_l ($\mu_l < \mu_r$) is the viscosity of the displacing fluid, U is the constant displacement velocity of the flow, T is the interfacial tension at the front, and k is the wave number. Thus interfacial tension T provides a cutoff wave number beyond which growth rate σ is negative. The maximum growth rate σ_{sm} and the corresponding dangerous wave number k_{sm} are given by

$$\sigma_{sm} = \frac{2(\mu_r - \mu_l)U}{3(\mu_r + \mu_l)} k_{sm}, \quad k_{sm} = \frac{1}{\sqrt{3}} \sqrt{\frac{(\mu_r - \mu_l)U}{T}}. \tag{2}$$

These formulae imply that increasing the interfacial tension or decreasing the positive viscosity jump at the interface can suppress instability. However, interfacial tension can reduce the instability only to some extent which is not sufficient to improve the oil recovery. In order to contain this instability to a meaningful level before breakthrough, various tertiary displacement processes are employed (see Pope 1980; Fayers 1981; Daripa and Pasa 2004). The simplest way to design such an EOR process is to use a layer of third fluid in between displaced and displacing fluids. This middle layer fluid can have either a constant viscosity μ with $\mu_l \leq \mu \leq \mu_r$ or a viscous profile $\mu(x)$ with $\mu_l \leq \min_x \mu(x) \leq \max_x \mu(x) \leq \mu_r$. According to (1), this makes each of these fronts less unstable individually due to reduction in the viscosity jump across each of them, assuming interfacial tensions at each of the fronts same as the one for the only front in the secondary recovery and ignoring any interaction between fronts. However, it must be stressed that the primary goal of this EOR process is stabilization of the leading front (i.e., the front sweeping the displacing fluid (oil) ahead). When the middle layer has non-constant viscous profile $\mu(x)$ with $\mu'(x) > 0$ even at a point, the middle-layer is also unstable (Daripa and Hwang 2008). Ideally, the viscous profile should be formulated so that this middle-layer instability does not offset the desired stabilization of the leading front in this EOR process. This middle-layer fluid is usually an aqueous phase (to be called polysolution henceforth) containing water and polymer in appropriate proportion to have the desired viscous profile. Since polymer is expensive, injection of polysolution is usually followed by injection of pure water to keep the cost low so that the recovery process is economically more viable. Many aspects of this three-layer flooding process, called polymer-flooding process, and multi-layer flooding process involving many piecewise constant viscous profiles have been studied by various authors. Below we briefly review as well as comment on some of these works so that contribution of the present work is properly placed within this broad EOR field.

Slobod and Lestz (1960) first experimentally studied the effect of two types of flooding process on stabilization in Hele-Shaw cell. First flooding process involved use of a sequence of polysolution having different constant viscosity with stepwise jump in viscosity at each of the fronts being positive in the direction of displacement. The study resulted in significant stabilization of the conventional Saffman–Taylor instability. This flooding process essentially involves multi-layer flow which was recently analyzed in great detail for Hele-Shaw flows by Daripa (2008a). This study by Daripa (2008a) not only obtained conditions necessary for the findings of Slobod and Lestz (1960) on stabilization to hold but also discovered

many features of this multi-layer flow such as an absolute upper bound on the growth rate of instabilities. The second flooding process (Slobod and Lestz 1960) studied involved use of a polysolution having a smooth monotonic viscous profile with viscosity increasing in the direction of displacement. This resulted in complete stabilization according to these authors. Mungan (1974) later also experimentally investigated the effect of this second flooding process on stabilization not only in Hele-Shaw cell but also in porous media. They also observed complete stabilization of the displacement process. This stabilization by this kind of graded exponential viscosity profile can not be explained by a theory based on the assumption of fluids involved being Newtonian (see Daripa and Hwang 2008). Perhaps, a theory based on the treatment of polysolution as a non-Newtonian fluid can explain this which is an open problem as of today.

The kind of exponential viscous profile that Mungan (1974) found to completely stabilize the flow was not economically viable. Uzoigwe et al. (1974) carried out two-dimensional numerical simulations with many economically viable viscous profiles of the polysolution. Their extensive numerical study led to the conclusion that the best policy of polymer injection corresponds to viscosity of the polysolution being close to the viscosity of displaced fluid (oil) at the leading front and decreasing exponentially back of the front to that of water (which corresponds to zero concentration of polymer) over a finite length. Many experimental studies documented in Littman (1998) and Sorbie (1991) support the idea that an exponential profile is perhaps economically more appropriate. Towards this end, the work of Needham and Doe (1987) should also be cited.

Pearson (1977) later first formulated the linear stability problem for the three-layer set up in which the middle layer has a variable viscous profile behind the advancing front. He studied stabilization of linear and exponential viscous profiles and concluded in favor of the exponential profile for stabilization. Using this linear stability formulation, later Gorell and Homsy (1983) studied the optimal injection policy of a fixed amount of solute under the constraint that the viscous profile behind the front can have a jump at the advancing front but the concentration of polymer must go to zero over a finite distance L (L depends on injection policy of polymer) behind the front. Thus, this set up has only one front which is displacing the oil ahead. Their study obtained results which were consistent with the earlier experimental results of Slobod and Lestz (1960) and Mungan (1974).

The following features of their injection policy were demonstrated numerically in Gorell and Homsy (1983): (i) the optimal viscous profile created by the injection of polymer need not have viscosity match at the advancing front. A physical explanation for the possibility of this finding is warranted which we provide here. Instability of the internal layer depends on the $\max_x \mu(x)$ where $\mu(x)$ is the viscous profile of the displacing fluid. In the set up of these authors, smaller the jump in viscosity at the advancing front, higher would be the value of the $\max_x \mu(x)$, i.e., less unstable the advancing front individually, more unstable is the displacing fluid layer individually. Therefore, it is not so hard to imagine based on the competition of these two instabilities that a distinct possibility exists of an optimal profile of the type obtained numerically by Gorell and Homsy (1983) that supports a finite jump in viscosity at the advancing front; (ii) the optimal viscous profile behind the advancing front is linear for small amount of solute (equivalently for small L) and is exponential for large amount of solute (equivalently for large L). This fact had been demonstrated earlier also by the works of Mungan (1974) and Uzoigwe et al. (1974); (iii) stabilization (i.e., reduction in growth rate of instabilities) is more pronounced for large values of injected polymer which should be expected on intuitive ground. However, there is an effective range of injected amount of polymer with an upper threshold (dependent on the viscosity ratio of displaced fluid (oil) to that of displacing fluid (water)) below which gain in stabilization gradually decreases with

increasing amount of injected polymer. Above this threshold, the effect of polymer injection on stabilization wears out rapidly. This should also be expected on intuitive ground.

Later, a significant advance in this EOR process by polymer flooding was made by Daripa et al. (1988b). These authors mathematically modeled this process in actual porous media using Buckley-Leverett model. This resulted in a coupled nonlinear system of conservations laws and elliptic partial differential equations which were then solved by a front tracking method Glimm et al. (1983) in homogeneous and heterogeneous porous media and also in rectilinear geometry of the type of Hele-Shaw cell. The effect of the middle layer containing polymer on the stabilization of the advancing front was thus investigated full fledged into linear and nonlinear regimes. The formulation of these authors allowed studies of initial three-layer set-up having two fronts across which mobility (equivalent to viscosity in Hele-Shaw model) is usually discontinuous at t (time) > 0. Thus this set up is very general and inclusive of all special cases studied earlier with Hele-Shaw and porous media models. Many of the earlier findings from linear stability analysis and experiments by previous authors on advantages of exponential viscous profile behind the advancing front in Hele-Shaw model was confirmed qualitatively. This is because even though the initial polymer concentration could be constant in the middle layer, conservation laws allow mixing of oil with the aqueous phase (due to rarefaction waves) behind the advancing front in a macroscopic sense and thus allow development of an exponential viscous profile of finite width (which vary with time) between the leading and trailing fronts due to rarefaction waves. Many other features of this tertiary displacement process and data of practical interest to oil industry were obtained by these authors (see Daripa et al. 1986, 1988a,b).

Within past few years, the linear stability problem has been revisited and analyzed by Daripa (2008a,b, 2011) and Daripa and Pasa (2010, 2008, 2007, 2006, 2005a,b, 2004) in order to derive exact results that provide insight and are directly useful. Some of these theoretical results obtained are the following: (i) local and global upper bounds on the growth rate for three-layer and N-layer flows and their applications in the development of necessary conditions for stabilization (see Daripa and Pasa 2005a,b; Daripa 2008a), (ii) bounds on short and long waves (see Daripa 2011), (iii) effect of stabilization on the unstable bandwidth and transfer of instability mechanism among fronts in three-layer flows (see Daripa 2008b), (iv) effect of diffusion on stabilization (see Daripa and Pasa 2007) and so on. These authors also obtained other new results review of which is not appropriate here. Rather we direct the readers to the above references. It is important to emphasize that flows involving variable viscosity internal layers were more difficult to treat theoretically than the constant viscosity internal layers case. Theoretical progress, therefore, was limited in the later case.

In this paper, we investigate numerically three-layer flows that can provide insight into EOR processes by ASP flooding followed by water flooding. In this kind of flooding process, there will be a front separating the water phase and the ASP-fluid phase. This front will have non-zero interfacial tension because of presence of interfacial surfactant. Modeling of this flooding process will have two fronts separated by a constant distance, each having interfacial tension and jump in mobility across them. This is unlike the case treated earlier in Gorell and Homsy (1983) for the pure polymer flooding with polymer concentration going to zero behind the advancing front over a finite length and thus having no trailing front. For the simplest tertiary enhanced recovery process, the three-layer (two-front) case is more appropriate with the internal fluid layer having a prescribed viscous profile. There will be competition between the individual instabilities at each front and instability in the internal layer. The outcome of this competition on the stabilization of the leading front (front displacing the oil) can only be determined through careful numerical study which is one of the goals of this paper. Motivated by this, we specifically study following problem in this paper: Within the three-layer context

having two fronts and a viscous profile in the internal layer, we investigate the changes in the maximum growth rate for various viscous profiles (monotonic and non-monotonic) in the absence of diffusion of polymer and identify optimal viscous profiles under the constraint that the length of the middle layer is fixed but the net amount of polymer is dependent upon the viscous profile. The other parameters in the problem such as the viscosity of the fluids (oil and water) in extreme layers are fixed. Results obtained from numerical computation are succinctly presented and discussed in this paper including the numerical method. Our results will be analyzed and summarized after these have been presented in this paper.

This paper is laid out as follows. The mathematical model, along with the governing equations is described in Sect. 2. The eigenvalue problem is described in Sect. 3. The numerical procedure for the solution of the eigenvalue problem is discussed in Sect. 4. In Sect. 5, numerical results are presented and discussed for constant and variable viscosity profiles. Both monotonic and non-monotonic viscosity profile are considered. Section 6 summarizes the main results and findings.

2 Preliminaries

The displacement of oil by the injection of one or more fluid phases in porous media is best described macroscopically by the Buckley-Leverett model (Daripa et al. 1988b). The flow description in porous media in this model consists of Darcy's law and conservation laws of all fluid phases assuming mixing of oil with the fluid phases in a macroscopic sense even though microscopically these could be immiscible. The analysis of underlying conservations laws shows that this model under most general initial conditions allows an advancing front displacing the oil ahead. However, there is mixing of oil and the displacing fluid phase in a macroscopic sense at the back of this advancing front due to rarefaction waves behind the advancing front. In the context of initial three-layer set-up of porous media flow by ASP-flooding in which the oil is displaced by an aqueous phase containing these three chemicals (alkali, polymer, and surfactant) which in turn is displaced by injection of pure water, there will usually be two active fronts with interfacial tension across each front.

This ASP model is an extended version of pure polymer model which has been discussed in great detail including the system of PDEs and their numerical solution procedure in Daripa et al. (1988b). In this paper, we simplify this ASP-model to gain some insight into the effect of some important features of this model without any recourse to numerical solution of the associated nonlinear system of coupled PDEs. This new simplified model is still a three-layer model with two fronts except that the viscous profile at the back of the leading front in this model is not generated by rarefaction waves or by mixing of phases but rather by a prescribed concentration profile of polymer in the middle layer of the three-layer flow. The surfactant is assumed to be on fronts only and thus interfacial tensions at both fronts are important features of this flow. The effect of alkali can be safely ignored because of the presence of only interfacial surfactant. This simplified model retains following features of the original ASP-flooding in homogeneous porous media with uniform constant porosity and permeability: (i) variable viscous profile of the middle layer and (ii) non-zero interfacial tensions at both the fronts. The effects of these on the stabilization of flow are investigated numerically with a goal to identify optimal viscous profile in the middle layer of fixed length. These studies correspond to an injection policy for fixed duration with total amount of polymer being injected dependent on the viscous profile in the middle layer. Such studies are done here for the first time.

The above simplified model is thus a three-layer flow with two fronts taken to be at $x = 0$ and $x = -L$. Fluid upstream $x = -\infty$ is assumed to have a velocity $(U, 0)$. In the left-most layer, $-\infty < x \leq -L$, viscosity of the fluid (water usually) is a constant denoted by μ_1 and that of the fluid (oil usually) in the right-most layer, $x > 0$, is denoted by a constant μ_r. The middle layer of length L contains a fluid (to be called polysolution henceforth) of variable viscosity $\mu(x)$ ($\mu_1 < \mu(x) < \mu_r$). The interfacial tension at the leading front separating oil from polysolution is denoted by T, and that at the trailing front separating water from polysolution is denoted by S. The fluid flow in this three-layer model is described by the following governing equations in each of the three layers.

$$\nabla \cdot \mathbf{u} = 0, \quad \nabla p = -\mu \, \mathbf{u}, \quad \frac{D\mu}{Dt} = 0, \tag{3}$$

where $\nabla = \left(\frac{\partial}{\partial x}, \frac{\partial}{\partial y} \right)$ and $\frac{D}{Dt}$ is the material derivative. The first equation $(3)_1$ is the continuity equation for incompressible flow, the second equation $(3)_2$ is the Darcy's law (Darcy 1856), and the third equation $(3)_3$ is the advection equation for viscosity (Gorell and Homsy 1983; Daripa and Pasa 2005b). The last equation simply states that the polymer and hence the viscosity is simply advected by the fluid. Below, we refer this model as the Hele-Shaw model (see also Daripa 2008a,b; Gorell and Homsy 1983; Pearson 1977).

We briefly review from our earlier works (see Daripa 2008a; Daripa and Pasa 2005a) the formulation of the eigenvalue problem arising from linear stability analysis of the uniform flow followed by the description of a finite difference based numerical method from Daripa and Pasa (2005b). The numerical method will be implemented and thus the eigenvalue problem will be solved for relevant data such as the maximum growth rate for parameterized continuous families of monotonic and non-monotonic viscosity profiles with non-zero interfacial tensions at two fronts.

3 The Formulation

The above system (3) admits a simple basic solution, namely the whole fluid set-up moves with speed U in the x direction and the two interfaces, namely the one separating the left layer from the middle-layer and the other separating the right layer from the middle-layer, are planar, i.e., parallel to the y-axis (Fig. 1). The pressure corresponding to this basic solution is obtained by integrating $(3)_2$. In a frame moving with velocity $(U, 0)$, the above system is stationary along with two planar interfaces separating these three fluid layers, and the smooth viscous profile $\mu(x)$ of the middle-layer fluid satisfies $\mu_1 < \mu(x) < \mu_r$. Here and below, with slight abuse of notation, the same variable x is used in the moving reference frame. In linearized stability analysis by normal modes, disturbances (denoted by tilde variables below) in the moving reference frame are written in the form

$$(\widetilde{u}, \widetilde{v}, \widetilde{p}, \widetilde{\mu}) = (f(x), \psi(x), \phi(x), h(x))e^{(iky + \sigma t)} \tag{4}$$

where k is the wave number and σ is the growth rate. We then insert this disturbance form into the linearized disturbance equations obtained from (3) and also into the linearized dynamic and kinematic interfacial conditions (see Daripa and Pasa 2005a). After some algebraic manipulation, we obtain the following differential equation in terms of only the eigenfunction $f(x)$ and the first derivative of viscosity μ_x in the middle layer:

$$-(\mu f_x)_x + k^2 \mu f = \lambda k^2 U \mu_x f, \qquad x \in (-L, 0) \tag{5}$$
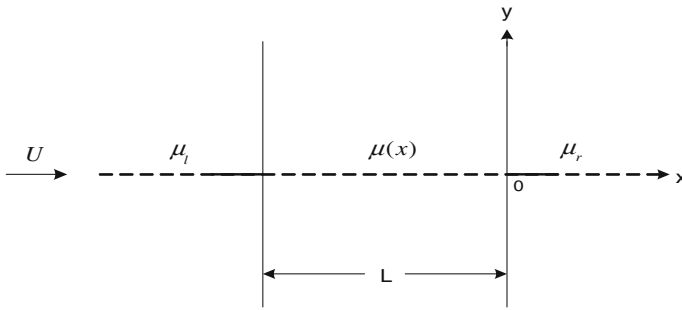
Fig. 1 Three-layer fluid flow

with boundary conditions

$$f_x(0) = (\lambda e + q)f(0), \qquad f_x(-L) = (\lambda r + s)f(-L), \tag{6}$$

where $\lambda = 1/\sigma$ and e, q, r, s are defined by

$$\left.\begin{aligned} e &= \{(\mu_\mathrm{r} - \mu(0))Uk^2 - Tk^4\}/\mu(0), \quad q = -\mu_\mathrm{r}k/\mu(0) \le 0, \\ r &= \{(\mu_1 - \mu(-L))Uk^2 + Sk^4\}/\mu(-L), \quad s = -\mu_1 k/\mu(-L) \ge 0. \end{aligned}\right\} \tag{7}$$

It should be mentioned here that the notation e above appears as notation p in some of our earlier works (e.g., see Daripa and Pasa 2005a) which we avoid using it here because the notion p we have used to denote pressure in this paper. When we consider that the intermediate region has a constant viscosity μ with $\mu_1 < \mu < \mu_\mathrm{r}$, problem (5) reduces to

$$\left.\begin{aligned} f_{xx} - k^2 f &= 0, \\ f_x(0) &= (\lambda e + q)f(0), \\ f_x(-L) &= (\lambda r + s)f(-L), \end{aligned}\right\} \tag{8}$$

where e, q, r, and s are the same as defined in Eq. (7) with $\mu(-L) = \mu(0) = \mu$, the constant viscosity of the middle layer.

4 A Numerical Method

For a given choice of values of T, S, U, L, μ_1, μ_r and the middle layer viscosity profile $\mu(x)$, the eigenvalue problem defined by (5), (6), and (7) will be solved by the numerical method presented below. Thus the $\max_k \sigma(k)$ from the dispersion relation $\sigma(k)$ for various viscous profiles is obtained numerically.

The eigenvalue problem is discretized using $(M-1)$ equidistant interior points in $(-L, 0)$: $x_M = -l < x_{M-1} < x_{M-2} < \ldots x_1 < x_0 = 0$, with $d = (x_i - x_{i+1})$. Using the first-order approximation for the end points derivatives and second-order approximation for the interior point derivatives namely,

$$\left.\begin{aligned} f_x(-L) &= (f_{M-1} - f_M)/d, \quad f_x(0) = (f_0 - f_1)/d, \\ f_x(y) &= [f(y + d/2) - f(y - d/2)]/d, \quad f_{xx}(y) = [f(y + d) - 2f(y) + f(y - d)]/d^2, \end{aligned}\right\} \tag{9}$$

where y is any one of the interior discretization points. Using these finite difference approximations (9) in the boundary conditions given in (6) and using the notation $f_i = f(x_i)$ leads to

$$(f_{M-1} - f_M)/d = (\lambda r + s) f_M, \quad (f_0 - f_1)/d = (\lambda e + q) f_0, \tag{10}$$

which are rewritten as

$$\frac{1}{rd} f_{M-1} - \left(\frac{1}{rd} + \frac{s}{r}\right) f_M = \lambda f_M, \quad \text{and} \quad \left(\frac{1}{de} - \frac{q}{e}\right) f_0 - \frac{1}{de} f_1 = \lambda f_0. \tag{11}$$

Using (9), (10), and (11) the discrete analog of the pde (5) together with the approximation (11) in a compact form is written as

$$A\overline{f} = \lambda B\overline{f}, \quad \overline{f} = (f_0, f_1, f_2, \ldots, f_M). \tag{12}$$

As an example, for the case of three interior points matrix A and B are given by

$$A = \begin{pmatrix} \left(\frac{1}{de} - \frac{q}{e}\right) & -\frac{1}{de} & 0 & 0 & 0 \\ \frac{-\mu_{1/2}}{d^2} & \left(\frac{\mu_{1/2}+\mu_{3/2}}{d^2} + \mu_1 k^2\right) & -\frac{\mu_{3/2}}{d^2} & 0 & 0 \\ 0 & -\frac{\mu_{3/2}}{d^2} & \left(\frac{\mu_{3/2}+\mu_{5/2}}{d^2} + \mu_2 k^2\right) & -\frac{\mu_{5/2}}{d^2} & 0 \\ 0 & 0 & -\frac{\mu_{5/2}}{d^2} & \left(\frac{\mu_{5/2}+\mu_{7/2}}{d^2} + \mu_3 k^2\right) & -\frac{\mu_{7/2}}{d^2} \\ 0 & 0 & 0 & \frac{1}{rd} & -\left(\frac{1}{dr} + \frac{s}{r}\right) \end{pmatrix} \tag{13}$$

$$B = \begin{pmatrix} 1 & 0 & 0 & 0 & 0 \\ 0 & k^2\beta\mu_1' & 0 & 0 & 0 \\ 0 & 0 & k^2\beta\mu_2' & 0 & 0 \\ 0 & 0 & 0 & k^2\beta\mu_3' & 0 \\ 0 & 0 & 0 & 0 & 1 \end{pmatrix} \tag{14}$$

where μ_i' denotes first derivative of $\mu(x)$ at point $x = x_i$. Similarly, $\mu_{i/2}$ stands for values of $\mu(x)$ at mid-point of of the subinterval $[x_{i-1}, x_i]$. We rewrite (12) as

$$C\overline{f} = \lambda\overline{f}, \quad C = (C_{ij}), \tag{15}$$

which for the case of three interior points is equivalent to multiplying the equations 2, 3, and 4 of system (12) by $(k^2\beta\mu_1')^{-1}$, $(k^2\beta\mu_r')^{-1}$, $(k^2\beta\mu_3')^{-1}$, respectively. It should be evident from matrices (13) and (14) that the above method is based on nested application of the first-order approximation for the first-order derivative term given in (9) to the first term of Eq. (5).

We have also solved the above problem defined by (5) and (6) by discretizing an alternate form of Eq. (5)

$$-\mu_x f_x - \mu f_{xx} + k^2\mu f = \lambda k^2 U \mu_x f \tag{16}$$

using the approximations given in (9) except for the first-order derivative term for which we now use the following second-order accurate approximation at the interior grid points such as y.

$$f_x(y) = \frac{f(y+d) - f(y-d)}{2d}. \tag{17}$$

This modification in the approximation improves the overall accuracy and yields the following discrete form of Eq. (5) at each interior grid point, $j = 1, \ldots, M-1$.

$$f_{j-1}\left(-\widetilde{k} - \frac{2\widetilde{k}\mu_j}{(\mu_x)_j d}\right) + f_j\left(\frac{4\widetilde{k}\mu_j}{(\mu_x)_j d} + \frac{\mu_j}{U(\mu_x)_j}\right) + f_{j+1}\left(\widetilde{k} - \frac{2\widetilde{k}\mu_j}{(\mu_x)_j d}\right) = \lambda f_j \tag{18}$$

where $\widetilde{k} = (2dk^2U)^{-1}$. With these approximations, the discrete analog of the problem takes a form similar to (15).

$$\widetilde{C}\,\overline{f} = \lambda \overline{f}, \qquad \overline{f} = (f_0, f_1, f_2, \ldots, f_M). \tag{19}$$

where $\widetilde{C}$ is a tri-banded square matrix of size $(M+1) \times (M+1)$. As an example, for the case of three interior points ($M = 4$), matrix $\widetilde{C}$ now is given by

$$\widetilde{C} = \begin{pmatrix} \left(\frac{1}{d\,e} - \frac{q}{e}\right) & \frac{-1}{d\,e} & 0 & 0 & 0 \\[2mm] -\widetilde{k}\left(1 + \frac{2\mu_1}{(\mu_x)_1 d}\right) & \widetilde{k}\left(\frac{4\mu_1}{(\mu_x)_1 d} + \frac{2dk^2\mu_1}{(\mu_x)_1}\right) & \widetilde{k}\left(1 - \frac{2\mu_1}{(\mu_x)_1 d}\right) & 0 & 0 \\[2mm] 0 & -\widetilde{k}\left(1 + \frac{2\mu_2}{(\mu_x)_2 d}\right) & \widetilde{k}\left(\frac{4\mu_2}{(\mu_x)_2 d} + \frac{2dk^2\mu_2}{(\mu_x)_2}\right) & \widetilde{k}\left(1 - \frac{2\mu_2}{(\mu_x)_2 d}\right) & 0 \\[2mm] 0 & 0 & -\widetilde{k}\left(1 + \frac{2\mu_3}{(\mu_x)_3 d}\right) & \widetilde{k}\left(\frac{4\mu_3}{(\mu_x)_3 d} + \frac{2dk^2\mu_3}{(\mu_x)_3}\right) & \widetilde{k}\left(1 - \frac{2\mu_3}{(\mu_x)_3 d}\right) \\[2mm] 0 & 0 & 0 & \frac{1}{dr} & -\left(\frac{1}{dr} + \frac{s}{r}\right) \end{pmatrix} \tag{20}$$

We have implemented the above two numerical methods. Both the methods yield the same results within machine accuracy. Using both the methods is more of a validation test of our results. All computations below are performed with $M = 30$. Conclusions made later concerning the optimal viscosity profile and other qualitative results have been found to be insensitive to increases in the value of M. These results are reported in the next section.

5 Numerical Results

In this section, we present numerical results for constant and variable viscosity profiles of the fluid in the middle layer with all other parameters of the problem fixed as follows: $T = 1, S = 1, U = 1, L = 1, \mu_1 = 2$, and $\mu_r = 10$. The goal is to seek an optimal viscosity profile $\mu(x)$, i.e., a viscous profile that gives the lowest value of the maximum growth rate over all possible disturbances. The viscous profiles over which this optimal viscous profile is sought numerically in this paper are constant viscosity profiles (see Sect. 5.1), monotonic viscous profiles of certain class (see Sect. 5.2), and non-monotonic viscous profiles of certain class (see Sect. 5.4).

5.1 Constant Viscosity Profile

We first consider the case when the middle layer has a constant viscosity μ with the constraint that $\mu_1 \leq \mu \leq \mu_r$. Then the system defined in Eqs. (5) and (6) reduces to a simpler form in (8) which has been solved analytically (Daripa 2008b) for the dispersion relations of two most dominant growth rates $\sigma_+(k)$ and $\sigma_-(k)$. In this section, we solve this constant viscosity-growth rates problem numerically using the finite difference scheme presented above and then compare with the exact results. This will also provide a verification that the numerical method produces the correct solutions.

The dispersion relations for the two smallest eigenvalues λ_1 and λ_2 are obtained using the finite-difference scheme. The corresponding two dominant growth rates are: $\sigma_1 = 1/\lambda_1$ and $\sigma_2 = 1/\lambda_2$. We find the number of mesh points $M = 30$ sufficiently large for the

Fig. 2 Constant viscosity case: Dispersion relationships—comparison between the numerically obtained growth rates σ_1 and σ_2 (*solid lines*) and analytically obtained growth rates σ_+ and σ_- (*dashed lines*). The parameter values are $\mu = 4, \mu_1 = 2, \mu_r = 10$, $T = S = U = 1$, and $L = 1$
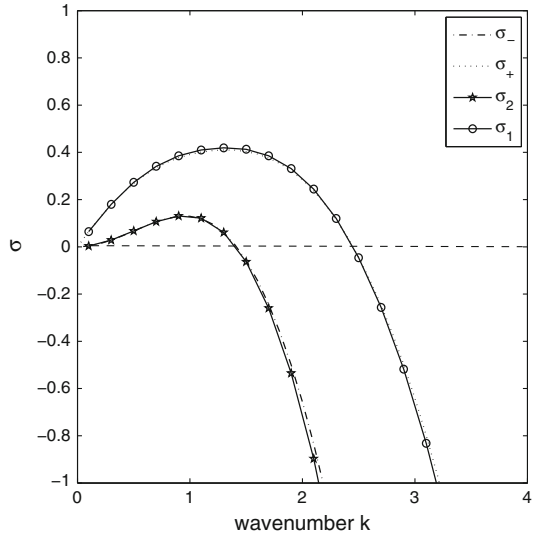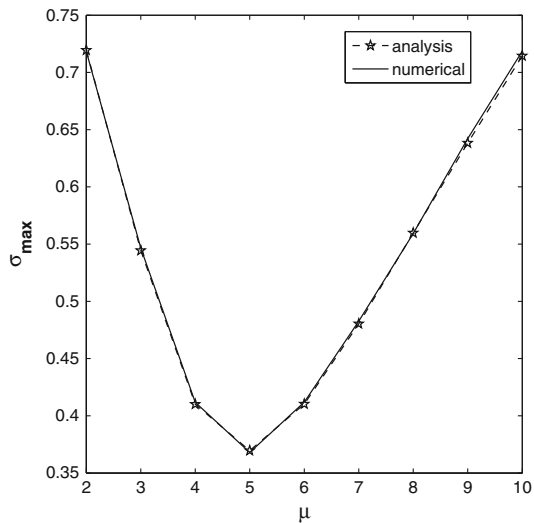
Fig. 3 Constant viscosity case:maximum growth rates σ_{max} versus μ. The other parameter values are fixed at $\mu_1 = 2, \mu_r = 10, T = S = U = 1$, and $L = 1$

convergence of the results when all the other parameters are same as in Daripa (2008b): $T = S = U = 1, L = 1, \mu_1 = 2, \mu_r = 10$, and $\mu = 4$. This also holds even when we use other values of these parameters. Figure 2 presents a comparison of the dispersion relations obtained from numerical computation and exact calculations presented in Daripa (2008b). The solid lines show computed growth rate σ_1 and σ_2, while the dashed lines display exact growth rates σ_+ and σ_-. It is clear that they agree very well.

Next we find the optimal constant viscosity μ from the window $\mu_1 \leq \mu \leq \mu_r$ that will minimize the maximum growth rate $\sigma_{max} = \max_k \sigma(k)$. Figure 3 compares the numerically obtained function $\sigma_{max}(\mu)$ (plot of σ_{max} vs μ) with exact solutions, respectively. Again the overall agreement is excellent. Furthermore, the results shown in this figure demonstrate that the smallest maximum growth rate σ_{max} for constant viscosity profile is approximately 0.3695

Fig. 4 Constant viscosity case:
maximum growth rates σ_{max}
versus length $1/L$ of the middle
layer when $\mu = 5$. The other
parameter values are
$\mu_l = 2$, $\mu_r = 10$,
$T = S = U = 1$,
and $L = 1$
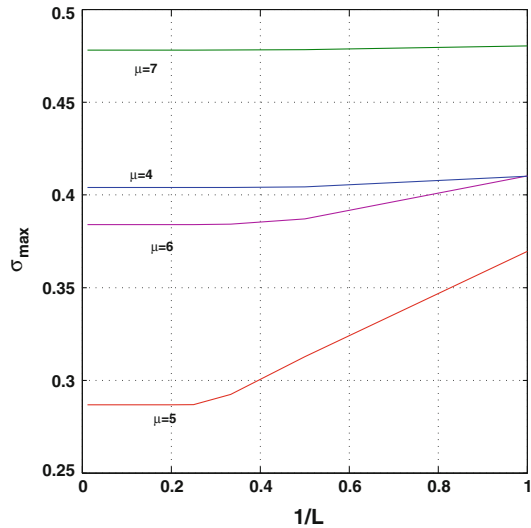
when the middle layer viscosity μ is 5. This is the optimal constant viscosity of the middle layer. Note this value may be different for different values of the parameters T, S, U, μ_1, and μ_r. However, the value of this optimal viscosity is independent of L with σ_{max} depending on L.

Figure 4 shows dependence of σ_{max} on $1/L$ for four representative values of μ. Of particular interest should be the plot for $\mu = 5$. It is found through studies of plots similar to Fig. 3 for many values of L that $\mu = 5$ is the optimal value for all these value of L. We find that σ_{max} for $\mu = 5$ approaches almost a constant value 0.286 for $1/L \leq 0.2$ and thus $\sigma_{max} \rightarrow 0.286$ as $L \rightarrow \infty$. We can also calculate this asymptotic value of σ_{max} theoretically as follows. In the limit $L \rightarrow \infty$, two fronts are far apart and individual maximum growth rate of the two fronts will not depend on each other. This maximum growth rate for each of the fronts is then given by Saffman–Taylor formula (2). Now if one were to compute this maximum growth rate using this formula for each of the two interfaces when $\mu = 5$, (for left interface use $\mu_r = 5$ and $\mu_1 = 2$ in formula (2); similarly, for the right interface use $\mu_r = 10$ and $\mu_1 = 5$ in formula (2)), one finds $\sigma_{sm} = 0.286$ for both the interfaces which agrees remarkably well with the numerical result. The rapid convergence for values of $L > 3$ that is seen in Fig. 4 is due to the fact that growth rates (see Daripa 2008b) depend weakly on L and decreases exponentially in L for large L.

5.2 Monotonic Viscosity Profile

We now turn our attention to the case of a smooth non-constant monotonic viscosity profile ($\mu_x \neq 0$) in the middle layer from certain families which are mentioned below. Our aim is to find general features of the viscosity profile $\mu(x)$ in the middle layer which maximizes the smallest eigenvalue λ, i.e., which minimizes the maximum growth rate σ_{max}. Four families of monotonic viscous profiles we consider are linear, exponential, sine, and polynomial. These viscosity profiles are shown in Fig. 5. These profiles are defined so that they have two end point viscosities $\mu(0)$ at $x = 0$ and $\mu(-L)$ at $x = -L$.
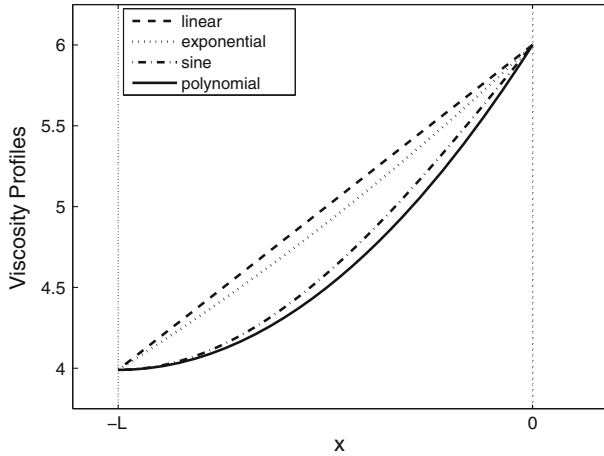
Fig. 5 Some examples of monotonic viscosity profiles in the middle layer when $\mu(-L) = 4$ and $\mu(0) = 6$

(1) Linear viscosity profiles:

$$\mu(x) = \frac{\mu(0) - \mu(-L)}{L} x + \mu(0), \quad -L < x < 0. \tag{21}$$

(ii) Exponential viscosity profiles:

$$\mu(x) = \mu(-L) \exp\{\alpha(x + L)\}, \quad \text{where } \alpha = \frac{1}{L} \ln \frac{\mu(0)}{\mu(-L)}. \tag{22}$$

(iii) Polynomial viscosity profiles:

$$\mu(x) = \frac{(\mu(0) - \mu(-L))}{L^2}(x + L)^2 + \mu(-L) \tag{23}$$

(iv) Sine viscosity profiles:

$$\mu(x) = (\mu(0) - \mu(-L)) \sin\left(\frac{\pi x}{2L}\right) + \mu(0). \tag{24}$$

Note that the constant viscosity profile is a special case of the above sine profile when $\mu(0) = \mu(L)$,

We recall the dimensional parameters of the problem: namely μ_l, μ_r, T, S, U, and L. In all our computations below we have used $T = S = U = 1$. Unless otherwise indicated or obvious from presentation of results, we have used mostly $\mu_l = 2, \mu_r = 10, L = 1$. Maximum growth rate is computed for all the above viscous profiles with $\mu(-L)$ and $\mu(0)$ varying in the range $[\mu_l, \mu_r]$.

In general, reduction in the viscosity jump across an interface is stabilizing individually to that interface. Similarly, a decrease in the maximum value of the gradient of the viscous profile is also individually stabilizing for the middle layer. Collective effects of all these instabilities determine the maximum growth rate for a specific viscous profile. Changing either $\mu(-L)$ or $\mu(0)$ or both within any one of the above four viscous family changes the severity of all these individual layer and interfacial instabilities. Therefore, computations are performed to find the optimal viscous profile even within a specific family (i.e., linear, exponential, sine, or polynomial) for which $\sigma_{\max}$ will be minimum. The results of such computations for linear and exponential viscous families are shown in Fig. 6a, b, respectively (for other two profiles,
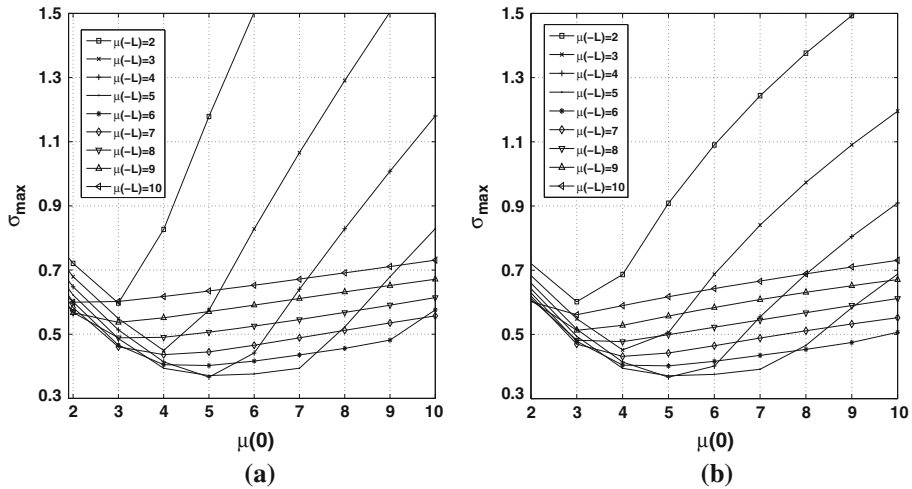
Fig. 6 Growth rate σ_{max} versus $\mu(0)$ for various values of $\mu(-L)$ when $\mu_l = 2$, $\mu_r = 10$, $T = S = U = 1$, and $L = 1$. **a** Linear profile. **b** Exponential profile

results are similar and not shown for brevity). This figure displays σ_{max} as a function of $\mu(0)$ for different values of the parameter $\mu(-L)$ for these two profiles. From Fig. 6a, following inferences can be drawn among many others.

- With increasing $\mu(-L)$, σ_{max} decreases when $\mu(-L) \leq 4$ (approximate). Thereafter for $\mu(-L) > 5$ (approximate), σ_{max} increases.
- For each constant $\mu(-L)$ curve, a value of $\mu(0)$ corresponding to the smallest value of σ_{max} is identified. From this, we find that minimum σ_{max} over all linear profiles is approximately 0.3652 when $\mu(-L) = 4$ and $\mu(0) = 5$. This is the most optimal one among all linear profiles. Note that this optimal linear profile allow all three entities (the layer and the two interfaces) to be individually unstable because of positive slope of the viscous profile and the positive jumps (in the direction of flow) across both the interfaces. Interestingly, note that this optimal linear profile is slightly more stabilizing than the optimal constant viscosity profile which has the maximum growth rate $\sigma_{max} = 0.3695$ when $\mu = 5$ (see Sect. 5.1).
- The linear viscous profile with no jumps in viscosity at the both the interfaces (i.e., the one for which $\mu(-L) = \mu_l$ and $\mu(0) = \mu_r$) gives the largest value of σ_{max}. This linear profile is the most destabilizing of all linear profiles.
- Among the linear profiles with no jump in viscosity at the left interface at $x = -L$, the most stabilizing one has $\sigma_{max} = 0.6$ (approximately) and $\mu(0) = 3$, thus allowing significant jump in viscosity at the right interface.
- Among the linear profiles with no jump in viscosity at the right interface at $x = 0$, the most stabilizing one has $\sigma_{max} = 0.55$ (approximately) and $\mu(-L) = 7$, thus allowing significant jump in viscosity at the left interface.

The inferences from Fig. 6a for exponential profile and from similar figures for sine and polynomial viscous profiles are similar to what we have observed for the linear case including the itemized inferences listed above for the linear profile. The main difference between these four families of viscous profiles are specific values of σ_{max}, $\mu(-L)$, and $\mu(0)$ for the optimal viscous profiles, one set for each family (linear, polynomial, sine, exponential). For example,

Fig. 7 Optimal monotonic viscosity profiles when $\mu_1 = 2$, $\mu_r = 10$, $T = S = U = 1$, and $L = 1$. This is a color plot on screen
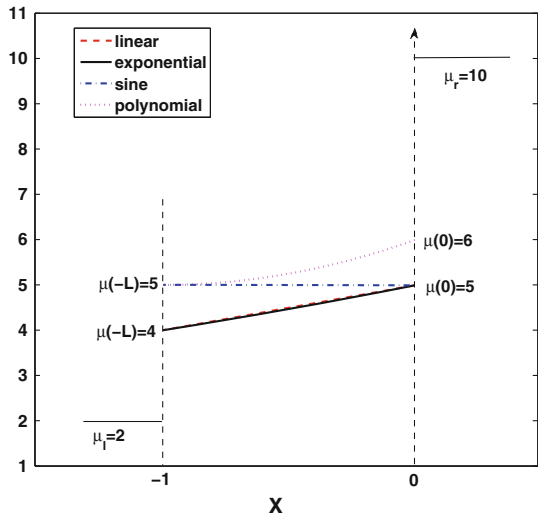
the optimal exponential profile has $\sigma_{max} = 0.3659$, $\mu(-L) = 4$, and $\mu(0) = 5$, optimal sine profile has $\sigma_{max} = 0.3695$, $\mu(-L) = 5$, and $\mu(0) = 5$ and optimal polynomial profile has $\sigma_{max} = 0.3678$, $\mu(-L) = 5$, and $\mu(0) = 6$. However, the general trend among all these profiles are same such as the optimal profile from each family has positive viscosity jumps across each interface, the most unstable profile from each family has no viscosity jumps at the interfaces and so on.

Recapping the values of σ_{max} which are 0.3695, 0.3652, 0.3659, 0.3695, and 0.3678 for optimal constant, optimal linear, optimal exponential, optimal sine, and optimal polynomial profiles, respectively. Thus, we see that influence of all these optimal profiles on σ_{max} is really small—in fact they are same up to two decimal digits. However, we see that the optimal linear profile is the most optimal one among all these variable viscosity profiles. Within the accuracy of computation, optimal linear, and optimal exponential profiles can be considered almost equally stabilizing. It perhaps indicates that these optimal profiles are close to each other at least for this value of $L = 1$. Figure 7 shows all the four optimal profiles where we see that only linear and exponential profiles are very close to each other within the resolution of the plots. Notice that the optimal sine profile is the constant profile which is a special case of sine profile when $\mu(0) = \mu(-L)$.

Figure 8 presents the relationship between $\mu(-L)$, $\mu(0)$ and the maximum growth rate σ_{max} in a square grid mesh, for the same parameters used above. The color for each grid cell is corresponding to value of the maximum growth rate σ_{max}, which can be read from the color bar. The coordinates of each cell location are related to $\mu(0)$ and $\mu(-L)$, respectively. The square cells on the diagonal line are corresponding to the constant viscosity profile case since $\mu(-L) = \mu(0)$. The cells below the diagonal line correspond to the cases when $\mu(-L) < \mu(0)$, and the cells up this line are related the profile where $\mu(-L) > \mu(0)$. The plot demonstrates that there exists a regime for $4 \leq \mu(-L) \leq 6$ and $4 \leq \mu(0) \leq 7$, in which the profile is more stable than other values of $\mu(-L)$ and $\mu(0)$.

Above results hold for $L = 1$. It is possible that optimal profile within each family as well as the optimal profile within all these four monotonic profiles may depend on L. We have explored this issue. Figure 9a, b shows plots of σ_{max} versus L for all four optimal profiles.
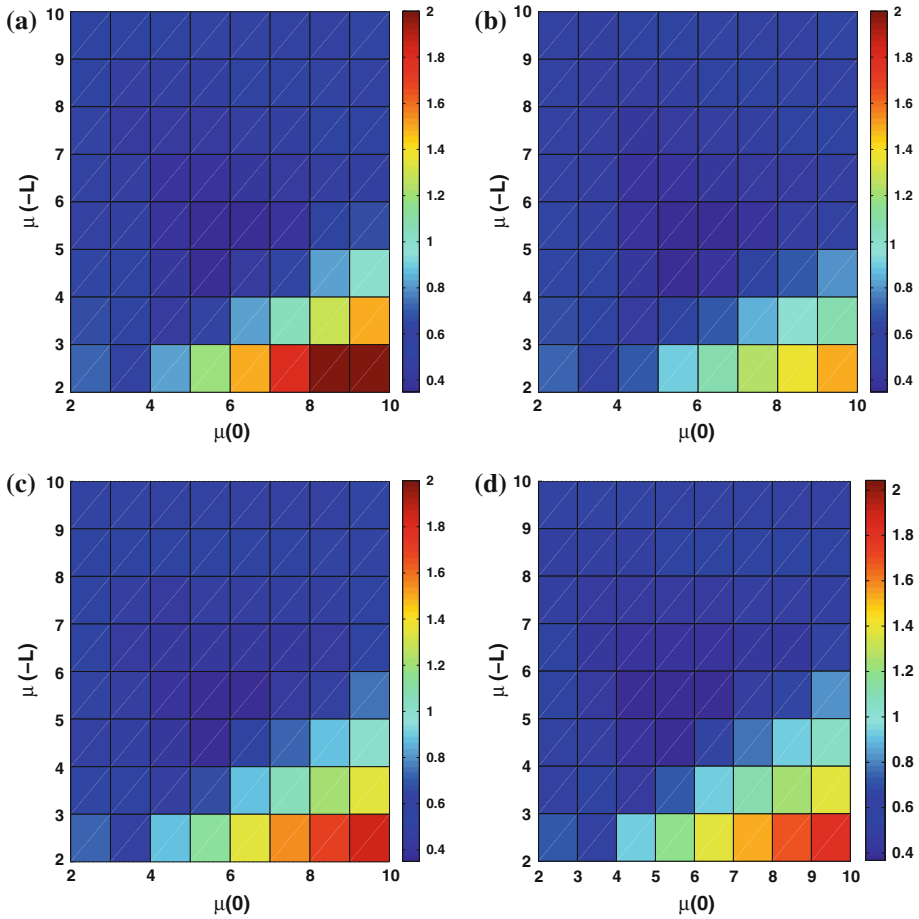
Fig. 8 Grid plot of $\sigma_{\max}$ as function of $\mu(-L)$ and $\mu(0)$ for monotonic viscosity profiles: **a** linear profile, **b** exponential profile, **c** sine profile, and **d** polynomial profile. The other parameter values are $\mu_l = 2$, $\mu_r = 10$, $T = S = U = 1$, and $L = 1$. This is a color plot on screen

Figure 10 shows similar plots of $\sigma_{\max}$ but as a function of $1/L$. From these figures, we can draw several inferences some of which are

- Maximum growth rate $\sigma_{\max}$ of the optimal profile from each family decreases with increasing L and appears to approach almost zero as $L \to \infty$. This is interesting because it suggests that the optimal profile from each family is almost completely stabilizing as $L \to \infty$. In this asymptotic limit slope of the viscous profile goes to zero and hence the middle layer is stable. Therefore, we can safely conclude that the both the fronts must be individually stabilizing in this limit and hence the viscosity jump at each front must approach zero as $L \to 0$. This is supported by the plots in Fig. 11a, b which shows plots of $(\mu_r - \mu(0))$ and $(\mu(-L) - \mu_l)$ against L, respectively. It should be noted that maximum stabilization within each family for finite values of L is obtained when all three instabilities (frontal and layer) are present individually.
- There are values of L for which the optimal profiles from four families are almost equally optimal since the minimized maximum growth rates are almost same.
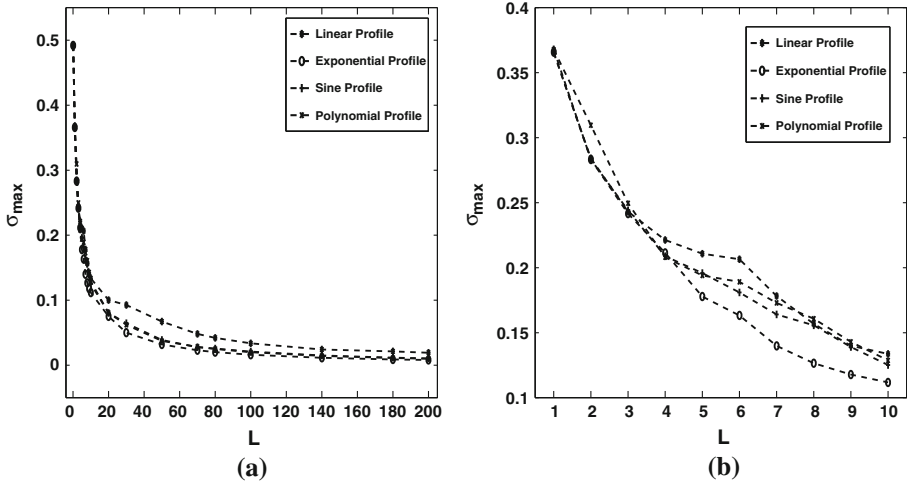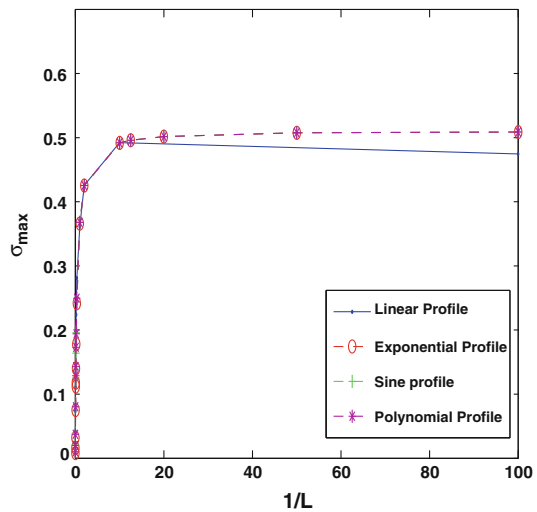
Fig. 9 Dependence of the maximum growth rate on L for optimal monotonic profiles. The upper most plot in **b** for $L < 3$ is for optimal polynomial profile. The other parameter values are $\mu_l = 2$, $\mu_r = 10$, and $T = S = U = 1$. **a** σ_{max} versus L. **b** Zooming in on the *left figure*

Fig. 10 σ_{max} versus $1/L$ for optimal monotonic profiles. The other parameter values are $\mu_l = 2$, $\mu_r = 10$, and $T = S = U = 1$. This is a color plot on screen

- Except for small values of $L < 1$ when optimal linear profile can be marginally better than exponentially, in general exponential optimal profile should be the choice among optimal profiles of all four families. It certainly is for higher ($L > 1$) but finite values of L. As we will see later, the exponential optimal profile also requires least amount of polymer among all four optimal profiles.

Since technically it is possible to improve oil recovery by controlling interfacial tensions using interfacial surfactants in displacing fluid, it is important to study stabilization potentials of optimal profiles at different interfacial tensions. This is what we do next. Figure 12a, b shows σ_{max} versus T and versus S, respectively, of the optimal profiles. For the leading front
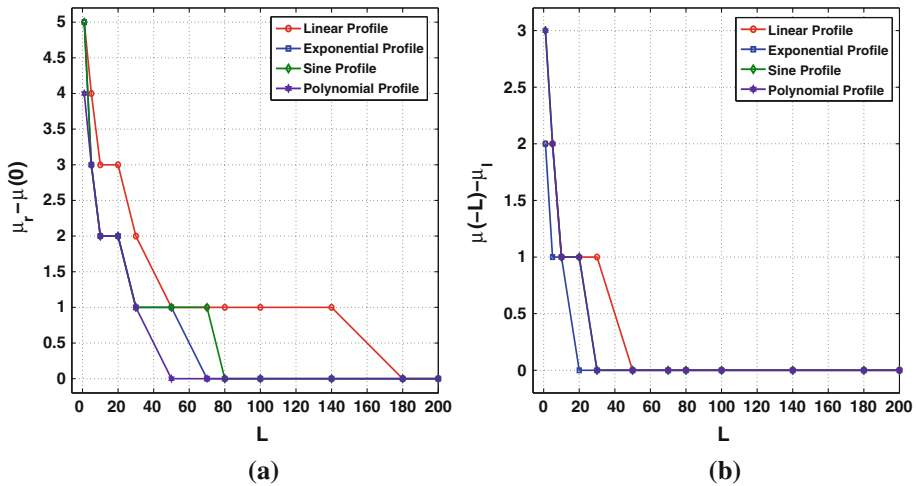
Fig. 11 Dependence of interfacial viscosity jumps for optimal monotonic profiles on the length of the middle layer. The other parameter values are $\mu_l = 2$, $\mu_r = 10$, and $T = S = U = 1$. **a** $(\mu_r - \mu(0))$ versus L. **b** $(\mu(-L) - \mu_l)$ versus L. This is a color plot on screen

with interfacial tension T, Fig. 12a shows that the most optimal profile is more or less the exponential optimal profile for all values of T except in a small window of T. In the figure, most optimal profiles for $T \leq 0.5$ (approximate value) and $T > 1$ (approximate value) are the optimal exponential ones. As T exceeds some value between 0.5 and 1, the most optimal profile is the linear one. It remains linear until T exceeds a value greater than but close to 1 when the most optimal profile clearly becomes the exponential one and remain so for increasing values of T. On line view of this figure when magnified will show this transition clearly on screen. We see that for values of $T > 4$ in the figure, difference between the four optimal profiles is hardly any. This figure shows that the optimal exponential profile is also the most stabilizing one of all profiles, though the differences between different optimal profiles are less than the one we observe in Fig. 12b for the leading or displacing interface for most values of S. These simulations provide only some understanding of the role of these optimal profiles on stabilization, though more simulations would be required to gain a full understanding of this issue for a choice of a specific optimal profile.

5.3 Optimal Viscous Profile for Pure Viscosity-Gradient Driven Instability

Viscous profiles with no jumps in viscosity (i.e., $\mu_r = \mu(0)$ and $\mu_l = \mu(-L)$) can cause instability if viscosity gradient $\mu_x > 0$ even at one point (see Daripa and Hwang (2008)). Such instabilities are pure viscosity-gradient driven. The normalized maximum growth rates for linear, exponential, polynomial, and sine profiles having no viscosity jumps at the interfaces are shown as functions of μ_r/μ_l in Fig. 13a when $L = 1$ and in Fig. 13b when $L = 10$. These results are based on computations with $T = S = U = 1$ and $\mu_l = 1$. The general observations enumerated below qualitatively remain intact even if a different value of μ_l is used.

The following few general observations can be made from the plots in this figure:

1. The flow becomes more and more unstable with increasing values of viscosity ratio ($\hat{\mu} = \mu_r/\mu_l$) for all four families of viscous profiles.
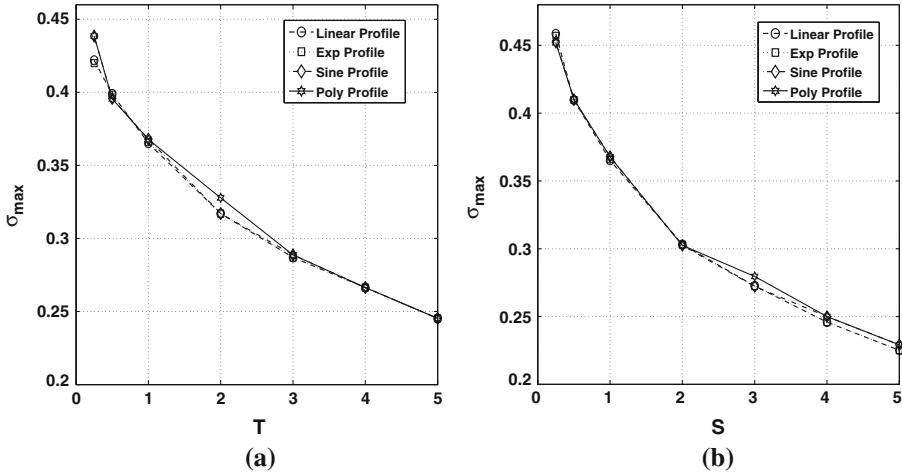
Fig. 12 Dependence of optimal monotonic profiles on interfacial tensions. Each point on the plots corresponds to an optimal profile. The other parameter values are $\mu_l = 2$, $\mu_r = 10$, and $U = L = 1$. Each optimal profile has its unique values of the pair ($\mu(-L)$ and $\mu(0)$). **a** σ_{max} versus T for optimal monotonic profiles when $S = 1$. **b** σ_{max} versus S for optimal monotonic profiles when $T = 1$
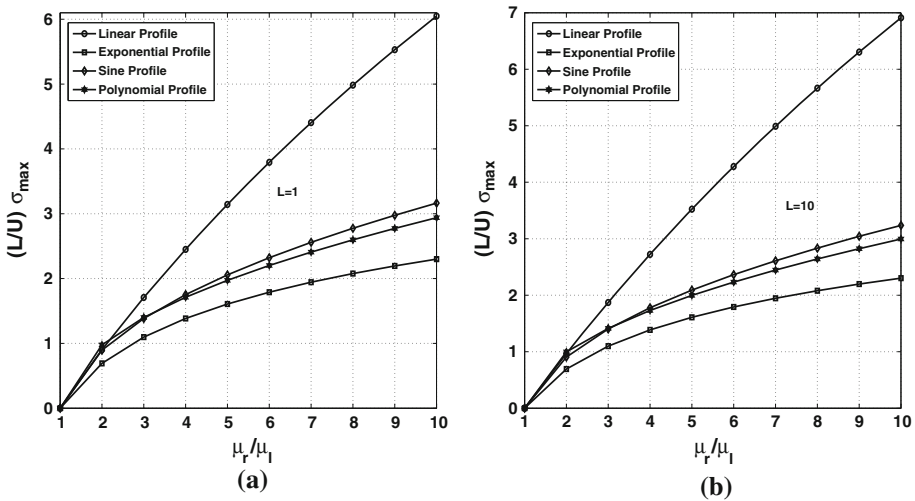

Fig. 13 Plots $(L/U) * \sigma_{max}$ for four viscosity profiles versus μ_r/μ_l for pure viscosity-gradient driven instability. σ_{max} is the maximum growth rate for the most optimal profile. The other parameter values are $T = S = U = 1$. **a** $L = 1$, **b** $L = 10$

2. Among the four profiles considered, the exponential profile is most stabilizing and the linear profile is least stabilizing for any value of $\hat{\mu} = \mu_r/\mu_l$. The figure shows data only in the range $1 < \hat{\mu} < 10$.

3. The linear, polynomial, and sine profiles are almost equally stabilizing for small values of $\hat{\mu}$ ($\hat{\mu} < 1.46$ in the figure when $L = 1$) but after a value, still small, of $\hat{\mu}$ ($\hat{\mu} \approx 3$ in the figure when $L = 1$), suddenly the sine and polynomial profiles become strongly

stabilizing in comparison to linear one for any fixed value of $\hat{\mu}$, with the polynomial one having slight edge over the sine one.

4. This figure shows that these above three characteristics hold for $L = 1$ and $L = 10$. In fact, this is true in general for all L in a qualitative sense. Interestingly, we have seen in Fig. 9 the above characteristics to hold for most optimal profiles from the four families (see Sect. 5.2) without the restriction of no jump in viscosity at the fronts.

It is important to recall from our discussion of the previous section that instability in the flow by all optimal profiles in Fig. 9a is driven by individual instabilities at both fronts and by viscosity-gradient driven instability in the middle layer.

5.3.1 Economics of Optimal Profiles

Since the most optimal profile from the four families for the purpose of maximum stabilization is the optimal exponential profile discussed earlier, it is useful to compare the costs involved in using the optimal profiles from these four families which we do next. We assume that viscous profile is created from adding polymer in small concentration in the fluid with viscosity μ_1.

For small polymer concentration C, the viscosity $\mu(C) = \mu_1(1 + \beta C)$, where the coefficient β is a polymer-dependent parameter. The concentration profile $C(x)$ for any viscous profile $\mu(x)$ integrated over the length L of the middle layer gives total amount of polymer $\beta C^T = (\int_{-L}^{0} \mu(x)\,dx - L)$. Thus, the total amount of polymers C_T^{lin}, C_T^{exp}, C_T^{poly}, and C_T^{sin} for the linear, exponential, polynomial, and sine viscous profiles are given by

$$\beta C_T^{\text{lin}}/L = \left(\tfrac{\hat{\mu}(0)+\hat{\mu}(-L)}{2} - 1\right), \qquad \beta C_T^{\text{exp}}/L = \left(\tfrac{\hat{\mu}(0)-\hat{\mu}(-L)}{\ln\hat{\mu}(0)-\ln\hat{\mu}(-L)} - 1\right),$$
$$\beta C_T^{\text{poly}}/L = \left(\tfrac{\hat{\mu}(0)+2\hat{\mu}(-L)}{3} - 1\right), \qquad \beta C_T^{\text{sin}}/L = \left(\tfrac{(\pi-2)\hat{\mu}(0)+2\hat{\mu}(-L)}{\pi} - 1\right). \tag{25}$$

where we recall that the variables with a hat in the above equation are normalized by μ_1. We define for purposes below the normalized amount of total polymer as $C_T^* = \beta C_T/L$. For the pure viscosity-gradient driven viscosity case when $\hat{\mu}(0) = \hat{\mu}_r$ and $\hat{\mu}(-L) = 1$, it then follows that for $\hat{\mu}_r \geq 1$ the normalized amount C_T^* of total polymer for various profiles are

$$\beta C_T^{\text{lin}}/L = \tfrac{1}{2}(\hat{\mu}_r - 1), \qquad \beta C_T^{\text{exp}}/L = \left(\tfrac{\hat{\mu}_r-1}{\ln\hat{\mu}_r} - 1\right),$$
$$\beta C_T^{\text{poly}}/L = \tfrac{1}{3}(\hat{\mu}_r - 1), \qquad \beta C_T^{\text{sin}}/L = \tfrac{\pi-2}{\pi}(\hat{\mu}_r - 1). \tag{26}$$

It then follows that $C_T^{\text{poly}} < C_T^{\text{sin}} < C_T^{\text{lin}}; \quad \hat{\mu}_r \geq 1$.

Figure 14a shows plots of normalized total polymer ($\beta C_T/L$) for exponential, linear, polynomial, and sine viscous profiles versus the viscosity ratio μ_r/μ_1 The following observations are made from these plots. The linear profile requires most polymer and thus most expensive compared to the other profiles. The total amount of polymer C_T for sine profile is between that for linear and polynomial profiles. The plots for exponential profiles cross these two plots, first the sine one at (5.6, 1.67) and then the polynomial one at (8.6, 2.53). Overall these three profiles (sine, poly, and exp) require more or less same amount of total polymer.

The following ratio is also of interest.

$$\frac{C_T^{\text{exp}}}{C_T^{\text{lin}}} = \left(\frac{\hat{\mu}_r - 1}{\ln\hat{\mu}_r} - 1\right)\left(\frac{2}{\hat{\mu}_r - 1}\right); \quad \hat{\mu}_r > 1. \tag{27}$$

The above ratio is a monotonically decreasing function of $\hat{\mu}$, meaning the amount of polymer needed for exponential profiles is less than that for linear profiles for all values of $\hat{\mu}_r$ so long
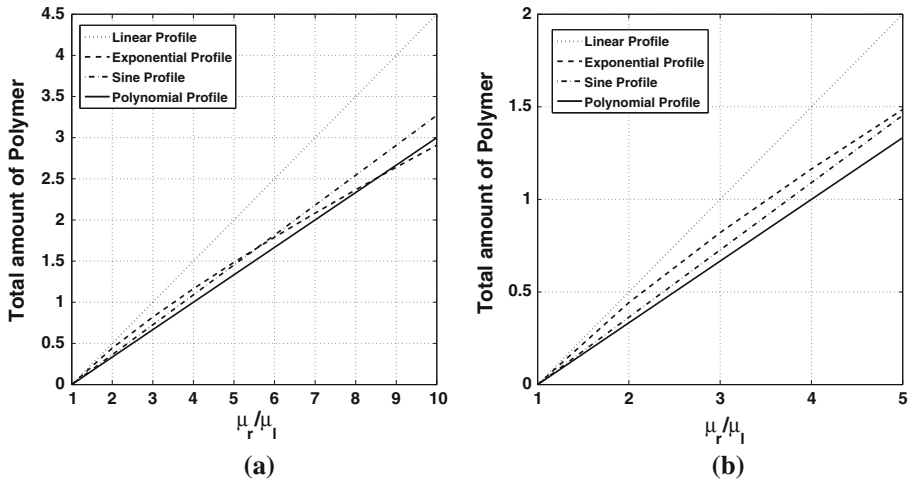
Fig. 14 Plots of normalized total polymer ($\beta C_T/L$) for exponential, linear, polynomial, and sine viscous profiles versus the viscosity ratio μ_r/μ_l for pure viscosity-gradient driven instability. **a** $L = 1$. **b** Magnified view of the *left corner* part of the figure on the *left*

as the extreme layer viscosities, upstream speed U and the length L of the intermediate layer remain same. Thus, the optimal exponential viscous profiles are not only are economical but also provide most stabilizing of all profiles. Figure 14a shows the relative merits of these two profiles as a function of $\hat{\mu}$.

5.4 Non-monotonic Viscosity Profile

For the case of monotonic viscosity profiles ($\mu_x > 0$), the layer itself was unstable and in the previous section we studied the interaction between individually unstable middle layer and individually unstable fronts in order to gain an understanding of the most optimal viscous profile within each family as well as the one among all four families of Sect. 5.2. In this section, we go one step beyond to find out if non-monotonic profiles in general can be more optimal than the most optimal one of the four families discussed above.

Every portion of the monotonic profile suffers instability because of positive (unfavorable) mobility gradient in the direction of basic flow. On the other hand, non-monotonic profiles introduce regions of favorable mobility gradient ($\mu_x \leq 0$) into the profile (see Fig. 15). This happens at the expense of steeper, in comparison to the monotonic case, unfavorable mobility gradient ($\mu_x > 0$) in some regions for the same total difference ($\mu(0) - \mu(-L)$) in mobility in the entire inner layer for both monotonic and non-monotonic profiles. Because of this, it is not obvious physically that the non-monotonic profiles will make the flow more or less stable in comparison to monotonic ones. It all depends on the profile and how the regions of favorable and unfavorable mobility gradients in the non-monotonic profile affect the overall fingering mode. So, it is physically obvious that non-monotonic profiles if properly designed can be more stabilizing than the most optimal non-monotonic profile. In general, it is not clear how to devise such profiles without formulating an associated inverse problem. However, given the experience of simulations reported above with monotonic profiles and with some intuition we are able to design some profiles which will show that non-monotonic profiles with better stabilizing properties do exist. In this section, we just do this by studying stabilizing capacity

Fig. 15 Some examples of non-monotonic viscosity profiles in the middle layer when $\mu(-L) = 4$ and $\mu(0) = 8$, where profile (0.3, exp) is $0.3\mu_1(x) + 0.7\mu_2(x)$ (exponential), profile (0.4,sine) is $0.4\mu_1(x) + 0.6\mu_2(x)$ (sine) and profile (0.3,poly) is $0.3\mu_1(x) + 0.7\mu_2(x)$ (polynomial)
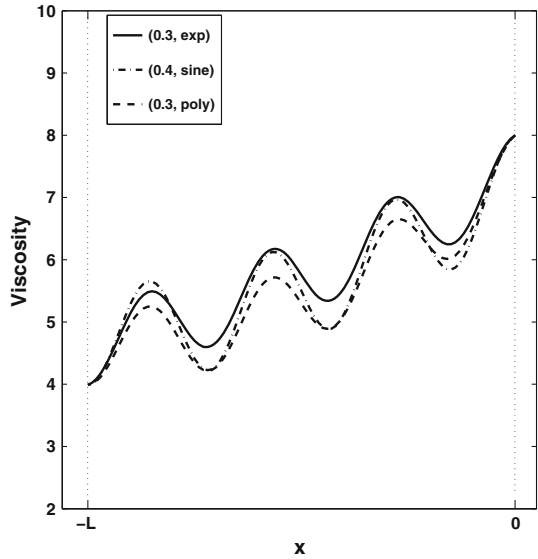
of some properly designed non-monotonic profiles and compare the results with the optimal monotonic profiles' results we have presented above.

One parameter families of non-monotonic viscosity profiles are constructed from any arbitrary monotonic profile of Sect. 5.2 using the formula

$$\mu(x) = \alpha\mu_1(x) + (1 - \alpha)\mu_2(x), \tag{28}$$

where

$$\mu_1(x) = \frac{\mu(0) - \mu(-L)}{2} \sin\left(7\pi\frac{x}{L} + \frac{\pi}{2}\right) + \frac{\mu(0) + \mu(-L)}{2}, \tag{29}$$

is a sine curve and $\mu_2(x)$ is any one of four monotonic profiles we defined in the last section, and α is a constant between [0,1]. The function $\mu(x)$ is defined so that the profile has the two end point viscosities $\mu(0)$ at $x = 0$ and $\mu(-L)$ at $x = -L$. Thus, non-monotonic viscous profiles constructed from (28) will be denoted by $(\alpha, \exp)$ when $\mu_2(x)$ in (28) is given exponential profile (22), and similarly by (α, poly) and $(\alpha, \sin)$ when $\mu_2(x)$ is given by polynomial profile (23) and sine profile (24), respectively. Figure 15 shows some examples of non-monotonic viscosity profiles.

Over the range of $\alpha \in [0, 1]$, and $\mu(-L), \mu(0) \in [\mu_1, \mu_r]$ for each family, the profile within each family which gives the smallest maximum growth rate and corresponding values of $\mu(-L), \mu(0)$ and α is found numerically for all three families of viscous profiles. Figure 16 shows these three optimal non-monotonic profiles. From plots $\sigma_{\max}$ versus $\mu(0)$ for values of viscosity $\mu(-L) \in [\mu_1, \mu_r]$ (not shown here), we find that $\sigma_{\max} = 0.3567$ for the most optimal (0.3,exp) profile which has $\mu(-L) = 4$ and $\mu(0) = 5$, $\sigma_{\max} = 0.3604$ for the most optimal (0.4,sine) profile which has $\mu(-L) = 5$ and $\mu(0) = 6$, and $\sigma_{\max} = 0.3618$ for the most optimal (0.3,poly) profile which has $\mu(-L) = 4$ and $\mu(0) = 5$. Thus the most optimal of all these non-monotonic profiles is the the profile (0.3,exp) with $\mu(-L) = 5$ and $\mu(0) = 6$ when $L = 1$, $S = T = U = 1$, the same parameter values used in Sect. 5.2. This optimal non-monotonic profile and in fact optimal profiles from all these three families

Fig. 16 Optimal non-monotonic viscosity profiles when $\mu_l = 2$, $\mu_r = 10$, $T = S = U = 1$, and $L = 1$. This is a color plot on screen
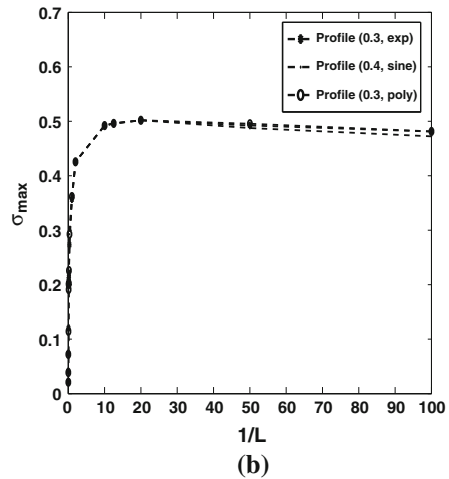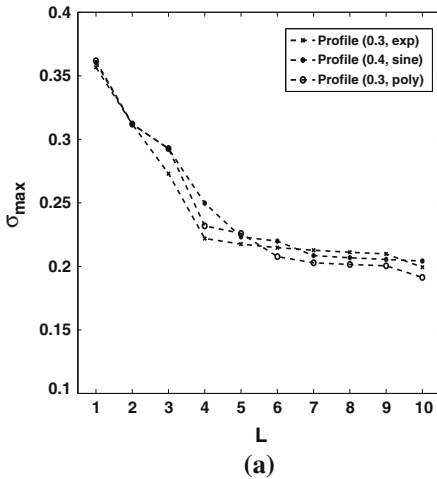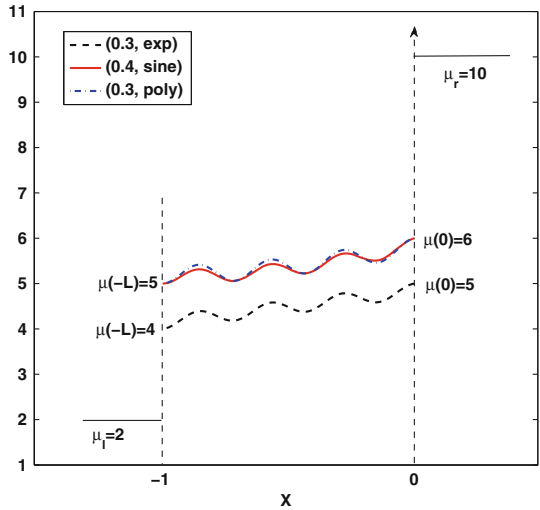

Fig. 17 Dependence of σ_{max} on L for optimal non-monotonic profiles from each of the three families of viscous profiles. The other parameter values are $\mu_l = 2$, $\mu_r = 10$, and $T = S = U = 1$. **a** σ_{max} versus L. **b** σ_{max} versus $1/L$

((0.3,exp), (0.4,sin), (0.3,poly)) have σ_{max} less than that for the most optimal monotonic profile for which $\sigma_{max} = 0.3659$ (see Sect. 5.2).

Above results for non-monotonic case were obtained when $L = 1$. In order to explore the effect of L on the selection of most optimal profile from these four families of viscous profiles, we have made simulations at several values of L in the range $[1, 200]$ for the same values of other parameters as before. Fig. 17a shows plots of σ_{max} versus L and Fig. 17b shows plots of σ_{max} versus $1/L$ for each of the three families of non-monotonic viscous profiles. The σ_{max} goes to zero as $L \to \infty$ but at a much slower rate than the case of optimal monotonic profiles.

Without flooding this paper with more figures, we just want to mention that for these optimal *non-monotonic profiles*, we have also done studies of dependence of interfacial viscosity
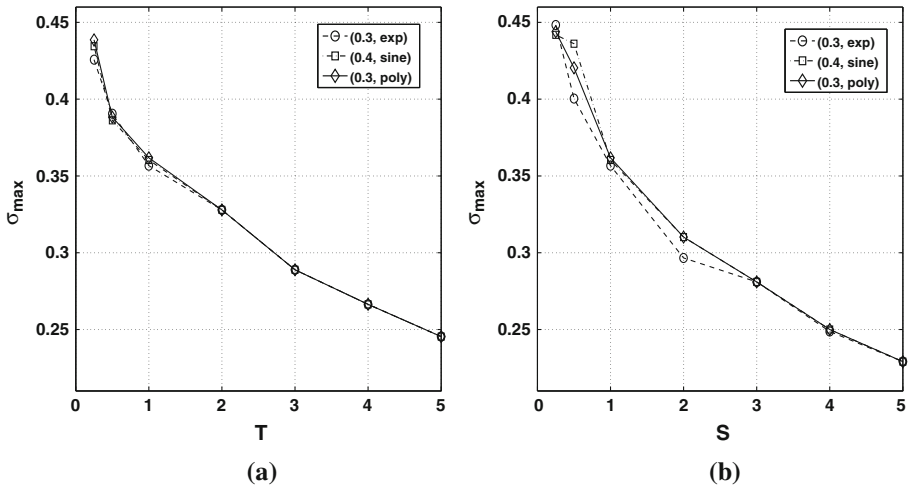
Fig. 18 Dependence of optimal non-monotonic profiles on interfacial tensions. Each point on the plots corresponds to an optimal profile. The other parameter values are $\mu_l = 2$, $\mu_r = 10$, and $U = 1$. Each optimal profile has its unique values of the pair $\mu(-L)$ and $\mu(0)$. **a** σ_{max} versus T for optimal non-monotonic profiles when $S = 1$. **b** σ_{max} versus S for optimal non-monotonic profiles when $T = 1$

jumps on L, similar to Fig. 11a, b for optimal monotonic profiles. Conclusions are similar: viscosity discontinuities ($\mu_r - \mu(0) \neq 0$ and $\mu_r - \mu(0) \neq 0$) at both the interfaces is a necessary condition for any fixed value of L. The viscosity jumps at both the interfaces decrease monotonically with increasing L and approach close to zero for a large enough L value of which depends on the optimal profile. However, they approach zero as $L \to \infty$ but at a much slower rate than the case of optimal monotonic profiles.

Like monotonic case (see Fig. 12a, b) discussed before, it is possible that the optimal non-monotonic profile does not remain within the same family (recall these families: (0.3,exp), (0.4,exp), (0.3,poly)) if interfacial tensions are changed. This is shown in Fig. 18a, b. Figure 18a shows that the most optimal profile is the (0.3,exp) profile for $T \leq 2$ (approx) and for $T > 2$, all optimal profiles of all three families are more or less equally optimal. Results of a similar study when instead interfacial tension S changes are shown in Fig. 18b.

5.5 Sensitivity to Interfacial Tension

Design of any flooding process should be tested for sensitivity to minor changes in the design parameter values. Such sensitivity studies are essential to robustness of the design. So, if a most optimal (say exponential) profile at some design conditions (i.e., for some choices of parameter values) is chosen, it is useful to know if it remains so under minor changes in parameter values, i.e., a study of parametric stability of the optimal profile is necessary. For purposes below, we define "$T = 1$" optimal profile of any family as the optimal profile of that family when interfacial tension $T = 1$.

We know that the maximum growth rate σ_{max} of the optimal profile should increase (decrease) with decrease (increase) in values of T, but we do not know the relative parametric stabilization capacity of the optimal profiles. Figure 19a, b exactly addresses this issue. This figure shows the sensitivity of the "$T = 1$" optimal profiles to changes in T from the design value $T = 1$. We recall that at $T = 1$ (with all other parameter values as the ones mentioned
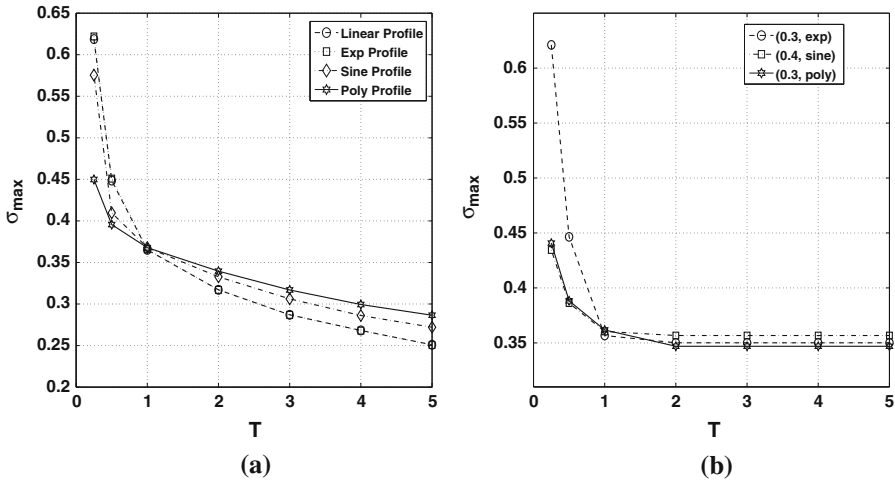
Fig. 19 Sensitivity of the optimal profiles: The dependence of σ_{max} of the "$T = 1$" optimal profiles on T. The other parameter values are $\mu_l = 2$, $\mu_r = 10$, and $S = U = 1$. The values of μ, $\mu(-L)$ & $\mu(0)$ for each optimal profile (corresponding to each curve/plot) has its unique values of the triple $(\mu(x), \mu(-L)$ and $\mu(0))$ at $T = 1$. **a** σ_{max} versus T for "$T = 1$" optimal monotonic profiles. **b** σ_{max} versus T for "$T = 1$" optimal non-monotonic profiles

in the figure caption), the most optimal profile is the exponential one among the monotonic profiles and the profile (0.3,exp) among the non-monotonic profiles. Figure 19a shows that even though the stabilization capacity increases (decreases) with increasing (decreasing) T, the exponential one loses its edge for values of $T < 1$ as the most stabilizing profile compared to others with the polynomial profile leading the group, followed by the sine profile, then the linear and the exponential ones finishing last having almost the same stabilizing capacity. Interestingly, for the non-monotonic case, Fig. 19b shows a different scenario: the (0.3,exp) profile remains the most optimal for values of T in approximate range [1.0, 1, 5), and for other values of T the (0.3,poly) takes the lead with (0.3,exp) closely following behind only for $T > 1.5$. Essentially, monotonic or not, the "$T = 1$" optimal exponential profile is not stable to changes in T. Interestingly, the stability of "$S = 1$" most optimal monotonic profile (which is linear) is very robust to small and large changes in the value of S as seen in Fig. 20a, On the other hand, Fig. 20b shows that the "$S = 1$" most optimal profile which is (03,exp) profile is stable to large and small changes in S so long as $S < 1.5$ (approximate). However, for $S > 1.5$ (approximate), (0.3,poly) takes the lead with (0.3,exp) closely following behind in stabilization.

6 Conclusions

In this paper, we have numerically studied an injection policy of tertiary recovery in porous media by ASP-flooding followed by water (or some other fluid of constant viscosity) flooding using Hele-Shaw model. This recovery process has been modeled here as a three-layer flow having the ASP-fluid that is displacing oil in the middle layer of finite length which is followed by a fluid such as water of constant viscosity. This corresponds to an injection policy over a fixed amount of time while the amount of polymer injected over a finite time may vary depending on the viscous profile. This is one distinction over the injection policy
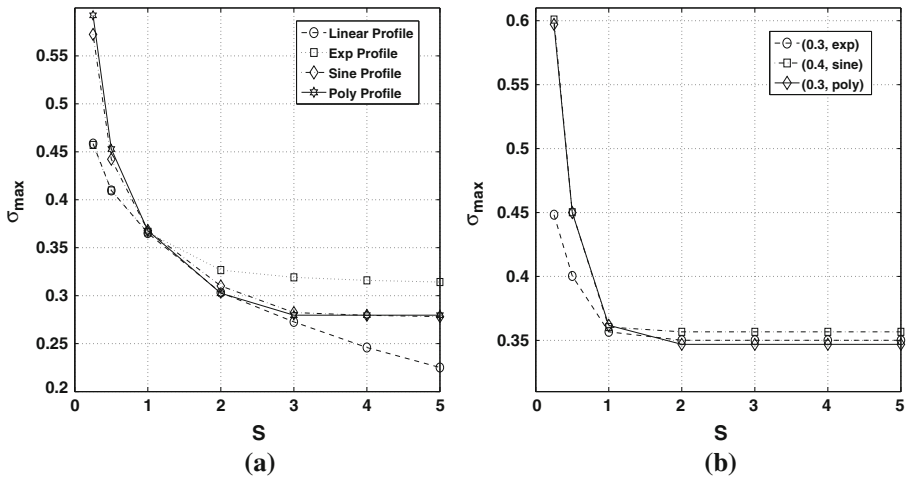
Fig. 20 Sensitivity of the optimal profiles: The dependence of σ_{max} of the "$S = 1$" optimal profiles on S. The other parameter values are $\mu_l = 2$, $\mu_r = 10$, and $T = U = 1$. The values of μ, $\mu(-L)$ and $\mu(0)$ for each optimal profile (corresponding to each curve/plot) has its unique values of the triple ($\mu(x)$, $\mu(-L)$ and $\mu(0)$) at $S = 1$. **a** σ_{max} versus S for monotonic profiles. **b** σ_{max} versus S for non-monotonic profiles

considered in Uzoigwe et al. (1974) and Gorell and Homsy (1983) in which the injected polymer is fixed but the duration over which it is injected (and hence the length over which the viscous profile is maintained) may vary. A second major difference is their consideration of only one front which is appropriate for secondary oil recovery processes and not for tertiary recovery processes. In contrast, we have considered in our study two fronts having non-zero interfacial tensions and possibility of finite viscosity jumps across these both fronts which is more relevant for the tertiary recovery process by ASP-flooding since surfactant is supposed to modify the interfacial tensions. This brings in added complication due to the presence of interfacial instabilities at both fronts unlike in the case of previous studies. The competition between three different types of individual instabilities, two interfacial modes and fingering (or layer) mode, determines the effectiveness of this injection policy. In contrast, mostly instability in the displacing fluid determines the effectiveness of the injection policy studied in the previous works of the above authors.

We have defined the meaning of an optimal profile from a family of viscous profiles. Numerically, we have identified optimal profiles from several viscous families and also identified the most optimal profile from a group of families of viscous profiles. We have considered four families (or functions) of monotonic viscous profiles and three families of non-monotonic viscous profiles. We have obtained several results on stabilization some of which are summarized below and, whenever possible, physical explanations for some of these findings are given.

1. For the constant viscosity case when L is not very small, optimal viscosity is the viscosity which gives the same growth rate for each of the two fronts based on the Saffman–Taylor formula. This finding is easily explained as follows. When L is large, the effect of one front on the other can be safely neglected (see Daripa 2008b). Maximum growth rates of each of the fronts can be calculated as functions of the middle layer fluid viscosity μ from the Saffman–Taylor formula. The viscosity at which these monotonic functions of viscosity intersect should be the optimal viscosity according to the definition, i.e.,

the viscosity at which the maximum of two growth rates is minimized. Basically, the interfacial modes split the difference $(\mu_r - \mu_1)$ so that neither of the interfacial growth rates dominate the other.

2. For optimal monotonic and non-monotonic viscous profiles of each family (linear, exponential, sine and polynomial), mobility jumps $(\mu_r - \mu(0) \neq 0$ and $\mu(-L) - \mu_1 \neq 0)$ at both the interfaces appear to be a necessary condition for any fixed value of L. The maximum growth rate σ_{max} and viscosity jumps at both the interfaces decrease monotonically with increasing L and approach close to zero for a large enough L value of which depends on the family of the optimal profile. But as $L \to \infty$, they approach zero. The above findings has the following rational explanation. In general, there is an interplay between the two interfacial modes and the fingering (instability in the layer) mode that determines the optimum viscous profile and associated viscosity jumps at two interfaces. Therefore, the optimum configuration (i.e., the interfacial viscosity jumps and the viscous profile in the layer) should result from splitting of the total mobility jump $(\mu_r - \mu_1)$ between the two interfacial modes and the fingering mode based on, loosely speaking, equidistribution of the instability between these modes so that highest maximum growth rate is smallest among all possible configurations. The signature of this argument is also seen in the dependence of the optimal configuration as L increases. With increasing L, mobility gradient of the profile and hence the fingering mode instability decrease unless the mobility jumps at interfaces also reduce with increasing L thus maintaining equidistribution of instability between all three modes. Therefore, results show that as $L \to \infty$, the mobility gradient of the profile as well as mobility jumps at interfaces approach zero.

3. The optimal linear profile is better than the other ones when width of the middle layer is small. With increasing values of L, the stabilizing capacity of the optimal exponential profile increases dramatically in comparison to other optimal profiles with the optimal linear profile doing the worst! Thus, for L not very small the optimal exponential profile is found to be the most optimal of all profiles. Increasing (decreasing) U with $L = 1$ has roughly same qualitative effect on relative standing of these optimal profiles as decreasing (increasing) L with $U = 1$. However, the effect of changing S and T can have dramatic effect on the optimality of these profiles.

4. Our results in general indicate that unless the width of the middle layer is very small, the most optimal profile is the exponential one, a result also supported by many petroleum engineering literature (Littman 1998; Mungan 1974; Needham and Doe 1987; Slobod and Lestz 1960; Sorbie 1991). The heuristic argument behind it is that the mobility gradient, expressed as a fractional mobility jump, is constant for an exponential, and therefore all portions of the profile suffer instability to the same degree. This argument assumes that the fingering mode does not depend on L which we have seen is true when L is not very small. When L is very small, the linear profile is seen to be optimal. This shows that the interplay of the three modes are strong when L is small and an approximate explanation as above based on superposition of the three instability modes does not apply.

5. Existence of non-monotonic profiles that can be less de-stabilizing than monotonic ones as expected on physical ground has been numerically confirmed from our limited studies in this paper. We have shown that all optimal non-monotonic profiles (linear (results not shown), exponential, sine, polynomial) are better than all optimal monotonic profiles for the purpose of stabilization.

6. For pure viscosity gradient driven instability, we have shown that the most optimal exponential viscous profile based on maximum stabilization capacity also requires least amount of polymer and hence is the best profile of choice.

7. There are similarities and dissimilarities in the results between the two injection policies: (i) The one studied here is for tertiary oil recovery and includes secondary recovery as a special case, whereas the one in GGorell and Homsy (1983) is for secondary recovery only. (ii) The one studied here numerically is based on constant time/length injection policy and the one studied in Gorell and Homsy (1983) theoretically is based on constant polymer injection policy. (iii) Both injection policies are studied using the Hele-Shaw model. (iv) Their study is restricted to only monotonic linear and exponential profiles. In contrast, our study considers wider families of viscous profiles including linear and exponential ones. Moreover, we have also investigated non-monotonic viscous profiles of these families. (v) In our injection policy, two fronts and interfacial tensions at both fronts exist which influence the outcome: characteristics of the optimal profile. Interestingly, the exponential (linear) profile becomes the profile of choice in both injection policies for large (very small) values of L. (vi) The crucial new effect in our injection policy is the interfacial tension at the trailing front and displacing front which can be modified due to surfactant. The results related to this is summarized next.

8. The most optimal profile designed for some choice of parameters can be unstable to changes in the parameter values such as interfacial tensions in the sense that changing the value of a design variable can make the profile from another family (such as switching from exponential to linear) the most optimal one.

In summary, the main contributions of the paper are that it (i) shows that the exponential profile is optimal over most of the parametric range and, when it is not, the growth rate of the optimal exponential profile is very close to that for the true optimum. In fact, there is little variation in the growth rates for all the profiles considered (with the possible exception of constant viscosity), (ii) establishes the dependence on parameters (interfacial tension, viscosity jumps, etc.), and (iii) existence of optimal non-monotonic profiles which are less unstable than the optimal monotonic ones.

In closing, it is worth mentioning that the basic flow considered is unidirectional and the parameters affecting stability in this study are slug size L, viscosity profile of the middle layer and interfacial tensions. The two-dimensional problem considered is in a plane perpendicular to gravity and therefore density or equivalently buoyancy effect does not appear in our treatment. Basic velocity U enters into the stability problem as a multiplicative factor with viscosity jumps at two interfaces (see Eq. (7)). Therefore, varying basic velocity U is equivalent to varying these viscosity jumps whose effect on the stability is well understood and can be interpreted from results presented in this paper.

References

Chouke, R.L., Van Meurs, P., VanDer Poel, C.: The stability of a slow, immiscible, viscous liquid–liquid displacements in a permeable media. Trans. AIME **216**, 188–194 (1959)

Darcy, H.: Les fontaines publiques de la ville de Dijon. Dalmont, Paris (1856)

Daripa, P.: Hydrodynamic stability of multi-layer Hele-Shaw flows. J. Stat. Mech. **12**, 28 (2008a)

Daripa, P.: Studies on stability in three-layer Hele-Shaw flows. Phys. Fluids. **20**, p. Article No. 112101 (2008b)

Daripa, P.: On estimates for short wave stability and long wave instability in 3-layer Hele-Shaw flows. Phys. A Stat. Mech. Appl. **390**, 3069–3076 (2011)

Daripa, P., Hwang, H.: Nonlinear Saffman–Taylor instability for Hele-Shaw flows. J. Diff. Equ. **245**(7), 1819–1837 (2008)

Daripa, P., Pasa, G.: An optimal viscosity profile in enhanced oil recovery by polymer flooding. Int. J. Eng. Sci. **42**, 2029–2039 (2004)

Daripa, P., Pasa, G.: New bounds for stabilizing Hele-Shaw flows. Appl. Math. Lett. **18**, 1293–1303 (2005a)

Daripa, P., Pasa, G.: On the growth rate for three-layer Hele-Shaw flows: Variable and constant viscosity cases. Int. J. Eng. Sci. **43**, 877–884 (2005b)

Daripa, P., Pasa, G.: A simple derivation of an upper bound in the presence of a viscosity gradient in three-layer Hele-Shaw flows. J. Stat. Mech. (2006). doi:10.1088/1742--5468/2006/01/P01014

Daripa, P., Pasa, G.: Stabilizing effect of diffusion in enhanced oil recovery and three-layer Hele-Shaw flows with viscosity gradient. Transp. Porous Med. **70**, 11–23 (2007)

Daripa, P., Pasa, G.: On capillary slowdown of fingering instability in immiscible displacement in porous media. Transp. Porous Med. **75**(1), 1–16 (2008)

Daripa, P., Pasa, G.: On diffusive slowdown in three-layer Hele-Shaw flows. Q. Appl. Math. **LXVIII**, 591–606 (2010)

Daripa, P., Glimm, J., Grove, J., Lindquist, B., McBryan, O.: Reservoir simulation by the method of front tracking. In: Proceedings of the IFE/SSI Seminar on Reservoir Description and Simulation with Emphasis on EOR, pp. 1–18 (1986)

Daripa, P., Glimm, J., Lindquist, B., Maesumi, M., McBryan, O.: On the simulation of heterogeneous petroleum reservoirs. In: Wheeler, M. (ed.) Numerical Simulation in Oil Recovery, IMA Vol. Math. Appl. 11, New York, NY, Springer, pp. 89–103 (1988a)

Daripa, P., Glimm, J., Lindquist, B., McBryan, O.: Polymer floods: a case study of nonlinear wave analysis and of instability control in tertiary oil recovery. SIAM J. Appl. Math. **48**, 353–373 (1988b)

Fayers, F. (ed.): Enhanced Oil Recovery. Elsevier, Amsterdam (1981)

Glimm, J., Lindquist, B., McBryan, O., Padmanabhan, L.: A front tracking reservoir simulator: 5-spot validation studies and the water coning problem. In: Frontiers in Applied Mathematics, vol. 1, Philadelphia, PA, Society for Industrial and Applied Mathematics (1983)

Gorell, S.B., Homsy, G.: A theory of the optimal policy of oil recovery by the secondary displacement process. SIAM J. Appl. Math. **43**, 79–98 (1983)

Littman, W.: Polymer Flooding: Developments in Petroleum Science. Elsevier, Amsterdam (1998)

Mungan, N.: Improved waterflooding through mobility control. Can. J. Chem. Eng. **49**, 32–37 (1974)

Needham, R.B., Doe, P.H.: Polymer flooding review. J. Petrol. Tech. **12**, 1503–1507 (1987)

Pearson, H.J.: The stability of some variable viscosity flows with application to oil extraction. Cambridge University Report (1977)

Pope, G.: The application of fractional flow theory to enhanced oil-recovery. Soc. Petrol. Eng. J. **20**, 191–205 (1980)

Saffman, P., Taylor, G.: The penetration of a fluid into a porous medium or Hele-Shaw cell containing a more viscous liquid. Proc. R. Soc. Lond. Ser. A **245**, 312–329 (1958)

Shah, D., Schecter, R. (eds.): Improved Oil Recovery by Surfactant and Polymer Flooding. Academic Press, New York (1977)

Slobod, R.L., Lestz, J.S.: Use of a graded viscosity zone to reduce fingering in miscible phase displacements. Producers Monthly **24**, 12–19 (1960)

Sorbie, K.S.: Polymer-Improved Oil Recovery. CRC Press, Boca Raton (1991)

Uzoigwe, A.C., Scanlon, F.C., Jewett, R.L.: Improvement in polymer flooding: The programmed slug and the polymer-conserving agent. J. Petrol. Technol. **26**, 33–41 (1974)